Thermal stability characterization of magnetic tunnel junctions using hard-axis magnetoresistance measurements

Pramey Upadhyaya,[1,a)] Pedram Khalili Amiri,[1] Alexey A. Kovalev,[2] Yaroslav Tserkovnyak,[2] Graham Rowlands,[3] Zhongming Zeng,[2] Ilya Krivorotov,[3] Hongwen Jiang,[2] and Kang L. Wang[1]
[1]*Department of Electrical Engineering, University of California, Los Angeles, California 90095, USA*
[2]*Department of Physics and Astronomy, University of California, Los Angeles, California 90095, USA*
[3]*Department of Physics and Astronomy, University of California, Irvine, California 92697, USA*

(Presented 17 November 2010; received 4 October 2010; accepted 27 October 2010; published online 23 March 2011)

The use of hard-axis magnetoresistance (MR) measurements for characterization of the device-level anisotropy field and thermal stability in CoFeB/MgO/CoFeB magnetic tunnel junctions is proposed and evaluated. We develop functional forms describing the hard-axis MR curves using a Stoner–Wohlfarth particle model, which are then used for fitting to the experimental curves to extract the free layer magnetic anisotropy field. The model accounts for nonidealities observed in the experimental MR curves in the form of asymmetry (with respect to applied fields), and linear drop in resistance at high fields. Micromagnetic simulations are used to identify the cause for these deviations and verify the presented model. © *2011 American Institute of Physics*. [doi:10.1063/1.3548830]

I. INTRODUCTION

Magnetoresistive random access memory driven by spin transfer torque (STT-MRAM) is a promising candidate for nonvolatile memory, owing to its high speed, endurance, and density, as well as better scalability compared to conventional MRAM.[1] The thermal stability factor ($\Delta = E/k_BT$) of a magnetic tunnel junction (MTJ) cell is an important performance metric of STT-MRAM, defining its data retention capability.[2] Here, E is the energy barrier between the two MTJ free layer states, k_B is the Boltzmann constant, and T is the operating temperature. The energy barrier (E) is in turn related to the device-level magnetic anisotropy field (H_k) of the free layer by $E = M_sH_kV/2$, where M_s is the saturation magnetization of the free layer and V is its volume, thus demanding an accurate measurement of H_k for thermal stability characterization of STT-MRAM. On the other hand, an accurate measurement of device-level anisotropy is a challenge due to the smaller amount of magnetic material compared to wafer-level measurements, which makes device-level tests prone to uncertainties due to thermal fluctuations and device-to-device shape variations. Methods used for H_k extraction include ferromagnetic resonance (FMR) (e.g., thermal, STT, or field-driven FMR measurements), where the existence of nonuniform modes complicates the data interpretation.[3,4] As well as in Stoner–Wohlfarth astroid measurements[5,6] where temperature and sweep rate dependence can result in a substantial deviation of the experimentally obtained curves from the ideal Stoner–Wohlfarth model.[7,8] In this work we propose the use of hard-axis magnetoresistance (HMR) curves for extraction of device-level anisotropy. Although HMR has the advantage of being both fast and least affected by temperature due to the absence of hysteresis, accurate characterization of H_k using this approach requires taking into account deviations such as possible misalignment in exchange bias and rotation of the fixed layer in response to the external field observed in the experimental data, making the hard-axis curves deviate from those expected from the Stoner–Wohlfarth model in the absence of these deviations (which we call the ideal model, see Fig. 1).

We review the major experimental features observed in HMR curves, identifying their causes, and devise a method to extract device-level H_k of the free layer from these curves. Section II presents and identifies the causes of typical deviations from the ideal model in measured curves using micromagnetic simulations. Based on this, a single-domain model is presented to derive functional forms for magnetoresistance in Sec. III, and is used in two limiting cases of low and high applied fields to extract H_k. The results are verified by comparison with anisotropy fields obtained from spin torque FMR (ST-FMR) and micromagnetic simulations.

II. EXPERIMENT AND SIMULATIONS

Magnetic tunnel junctions with a composition of PtMn (15 nm)/CoFe (2.5 nm)/Ru (0.85 nm)/CoFeB (2.4 nm)/MgO (~0.8 nm)/CoFeB (1.8 nm) were sputter deposited in a Singulus TIMARIS PVD system, followed by annealing in a field of 1 T at 300 °C for 2 h. The films were then patterned into elliptical nanopillars using electron beam lithography and ion milling. The MgO thickness was designed to result in a resistance-area product of ~3.5 Ω μm^2, which was verified through current-in-plane tunneling tests, as well as measurements on the patterned devices. Device-level magnetoresistance and FMR measurements were performed using a probe station in a one-port ground-signal–ground configuration. Figure 1(b) shows a typical HMR curve measured on a 130 nm × 50 nm MTJ pillar. It exhibits two features (circled) that are different from the ideal model: (i) Asymmetry with

a)Author to whom correspondence should be addressed. Electronic mail: prameyu@ucla.edu.

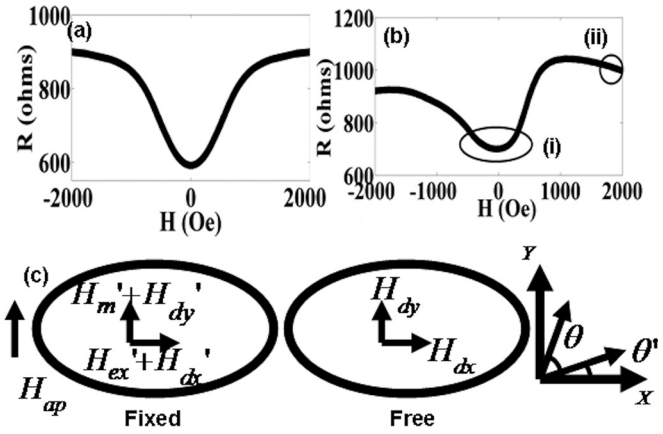

FIG. 1. (a) Ideal model: hard-axis curve using micromagnetic simulations for 130 nm × 50 nm MTJ with a fixed layer pinned by 10,000 Oe and no misalignment. (b) Measured resistance vs applied field curves for 130 nm × 50 nm MTJ along the hard axis, highlighting deviations from ideal curves in the form of (i) asymmetry of the MR curve and (ii) rotation of the fixed layer magnetization. (c) The model and the coordinate system used for deriving the fitting functions showing fixed and free layer magnetizations making an angle θ' and θ with respect to the easy axis. H_{ap} is the external applied field along hard axis, H'_{ex} is the exchange bias field from antiferromagnet, H'_m is the field due to misalignment of exchange bias, whereas H_{dx}, H'_{dx}, H_{dy}, and H'_{dy} represent the dipolar stray fields.

respect to applied fields and (ii) linear drop in resistance at high fields. These can be attributed to misalignment of the exchange bias field with respect to the easy axis, and rotation of the fixed layer magnetization at high fields, respectively, as described in the following.

We performed energy minimization using micromagnetic simulations[9] of an elliptical CoFeB/MgO/CoFeB MTJ structure with varying lateral dimensions (50 nm × 100 nm to 50 nm × 140 nm) for simulating the hard-axis loops. The effect of the antiferromagnetic PtMn film on the fixed layer was modeled by including a pinning exchange bias field (H'_{ex}). The parameters used in the simulations were free and fixed layer saturation magnetizations of 1000 and 1200 emu/cm^3, exchange stiffness in both fixed and free layers of 2×10^{-6} erg/cm, and lateral cell dimensions of 5 nm × 5 nm in each layer. The hard-axis field was varied between ± 2000 Oe. The asymmetry of the magnetoresistance curve was reproduced in the simulations by allowing for a misalignment in exchange bias, resulting in equilibrium magnetization of the fixed layer having an angle (<5° for all fitted curves) with the long (i.e., easy) axis of the ellipse. This was modeled in simulations by including an exchange bias field component along the hard axis of the fixed layer (H'_m), with the misalignment angle defined as $\theta = \tan^{-1}(H'_m/H'_{ex})$. On the other hand, a linear drop in resistance at high field was observed in simulations due to the in-plane rotation of the fixed layer toward the free layer (which is almost saturated along the hard axis at high fields). The slope of this drop depends on the value of the pinning field acting on the fixed layer.

III. MODEL AND DISCUSSION

Figure 1(c) schematically shows the model used for deriving the fitting functions. An external applied field (H_{ap}) acts along the hard axis (y axis) on both fixed and free layers. The exchange bias field acting on the fixed layer is denoted by H'_{ex} (along the pillar length), whereas H'_m accounts for the misalignment of exchange bias as discussed in the previous section. H_{dx}, H'_{dx}, H_{dy}, and H'_{dy} represent the dipolar stray fields along x and y axes on the free and fixed layers, respectively. Assuming single domain behavior and equilibrium magnetization lying in the x–y plane (i.e., Stoner particle behavior as verified from micromagnetic simulations), for an applied hard-axis field the effective field on free (H_{eff_free}) and fixed layers (H_{eff_fix}) is given by $H_{eff\_free} = (H_{dx} - N_x M_s \cos\theta)\hat{x} + (H_{ap} - N_y M_s \sin\theta + H_{dy})\hat{y}$ and $H_{eff\_fix} = (H'_{ex} - N'_x M_s \cos\theta' + H'_{dx})\hat{x} + (H_{ap} + H'_m - N'_y M_s \sin\theta' + H'_{dy})\hat{y}$, respectively. Here N_x, N'_x and N_y, N'_y are demagnetizing factors along x and y axes, and θ, θ' are equilibrium angles of the free and fixed layer magnetizations, respectively [Fig. 1(c)]. Equilibrium requires the effective field to align with the magnetization, which gives

$$\tan\theta = \frac{(H_{ap} + H_{dy} - N_y M_s \sin\theta)}{(H_{dx} - N_x M_s \cos\theta)}, \tag{1}$$

$$\tan\theta' = \frac{(H_{ap} + H'_{dy} + H'_m - N'_y M_s \sin\theta')}{(H'_{ex} + H'_{dx} - N'_x M_s \cos\theta')}. \tag{2}$$

The resistance of the MTJ is then given by

$$R = \frac{R_{ap} + R_p}{2}\left[1 - \frac{R_{ap} - R_p}{R_{ap} + R_p}(\cos\phi)\right], \tag{3}$$

where R_p and R_{ap} are the MTJ resistance in parallel and antiparallel states, respectively, and $\phi = \theta - \theta'$. In general, the dipolar fields between the layers for an arbitrary angle between fixed and free layers are unknowns, making it impossible to find a closed-form solution of Eqs. (1)–(3) for magnetoresistance. However, the dipolar fields can be approximated in two special limits of applied fields giving closed forms of the magnetoresistance as described in the following.

For small applied fields, the dipolar field on the free layer due to stray fields from the synthetic antiferromagnetic fixed layer is given by the shift in the easy axis hysteresis loop (H_s). The effect of the dipolar stray field of the free layer acting on the fixed layer can be neglected in comparison to the exchange bias field for a strongly exchange biased fixed layer (i.e., $H_{dx} \approx H_s$, $H_{dy} \approx H'_{dy} \approx 0$, $H'_{ex} \gg H'_{dx}$. Also, both θ and θ' are small (i.e. $\tan\theta \approx \sin\theta \approx \theta$), which, when substituted in Eqs. (1)–(3) yield

$$R(H_{ap}) = \frac{(R_p + R_{ap})}{2}\left[1 - \frac{(R_{ap} - R_p)}{(R_p + R_{ap})} \times \left\{\sqrt{\left(1 - \left(\frac{H'_m + H_{ap}}{H'_k}\right)^2\right)}\sqrt{\left(1 - \left(\frac{H_{ap}}{H_k + H_s}\right)^2\right)} + \left(\frac{H'_m + H_{ap}}{H'_k}\right)\left(\frac{H_{ap}}{H_k + H_s}\right)\right\}\right], \tag{4}$$

where free layer $H_k = (N_y - N_x)M_s$ and we define $H'_k = H'_{ex} + (N'_y - N'_x)M_s$.

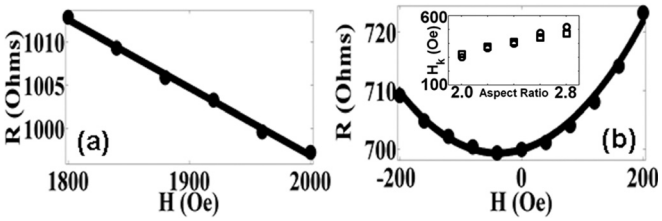

FIG. 2. Thermal stability extraction by fitting of measured hard-axis magnetoresistance curve to the derived functional forms for free layer H_k extraction: (a) Fit of Eq. (6) (for an elliptical 130 nm × 50 nm MTJ pillar) to the high-field region [marked as (ii) in Fig. 1(b)], giving $H'_k = 6663$ Oe, and (b) fit of Eq. (4) (for same MTJ pillar) to low-field region [marked as (i) in Fig. 1(b)], with dipolar field (H_s) obtained from the shift in easy-axis loop, giving free layer $H_k = 620$ Oe. Inset in (b) shows comparison of micromagnetic simulations of free layer anisotropy for five 50-nm-wide devices with different aspect ratios. Squares and circles indicate the values obtained from MH curves and HMR data, respectively.

In the limit of large applied fields [~2000 Oe in Fig. 1(b)], we observe a linear drop in resistance with increasing field. From micromagnetic simulations we observe that the free layer is almost saturated along the hard axis (i.e., $\theta \approx 90°$) in this range of fields, implying that the contribution of dipolar fields from free layer on the fixed layer along y axis cannot be neglected. However, dipolar contribution along the x axis of the fixed layer can still be neglected in comparison to the exchange bias field ($H'_{ex} \gg H'_{dx} \approx 0$, $H'_{dy} \neq 0$). Moreover, as the exchange fields on the fixed layer are much larger than the applied fields, a small angle approximation can still be used for the fixed layer (i.e. $\tan\theta' \approx \sin\theta' \approx \theta'$). Substituting these approximations into Eqs. (1)–(3), we have

$$R(H_{ap}) = \frac{R_p + R_{ap}}{2}\left(1 - \frac{R_{ap} - R_p}{R_p + R_{ap}}\left(\frac{H_{ap} + H'_m + H'_{dy}}{H'_k}\right)\right). \quad (5)$$

Thus, the slope of the linear drop in resistance at high fields is given by

$$dR/dH_{ap} = (R_{ap} - R_p)/(2H'_k). \quad (6)$$

An example of free layer H_k extraction using the aforementioned fitting functions on a measured hard-axis curve is shown in Fig. 2. In order to validate the method developed in this paper, we applied it to hard-axis curves calculated using micromagnetic simulations for varying aspect ratios (see Fig. 2 inset) with a free layer thickness of 1.8 nm. The free layer H_k was obtained from the simulations in two ways: (i) from simulated magnetization versus hard-axis field (M–H) for a single free layer and (ii) by fitting the simulated HMR curve, including the fixed, spacer, and free layers using Eq. (4). The parameters used were the same as mentioned in Sec. II with pinning field along the long axis of the fixed layer $H'_{ex} = 5000$ Oe, and the misalignment field along the hard axis of the fixed layer $H'_m = 400$ Oe for each device. The dipole fields (H_s) and the resistance values in parallel and antiparallel states required for using Eq. (4) were calculated by simulating the easy-axis loops (not shown). Figure 3 compares the free layer H_k extracted using M–H and HMR for various aspect ratios, showing a good agreement between the two approaches. We note that the disagreement between the two values increases with device size, indicating the role of nonuniformity of dipolar fields (which we have assumed to be uniform). The experimentally extracted H_k also showed agreement with ST-FMR results to within <5%, based on ST-FMR and HMR measurements on several nominally similar devices.

TABLE I. Thermal stability for MTJ nanopillars with varying dimensions, showing increase in thermal stability with area and aspect ratio.

Lateral dimensions	Area (μm^2)	Aspect ratio	Thermal stability factor
110 nm × 50 nm	0.0043	2.2	39
130 nm × 50 nm	0.0051	2.6	67
135 nm × 65 nm	0.0069	2.08	88
160 nm × 65 nm	0.0082	2.46	105
140 nm × 85 nm	0.0093	1.65	81
170 nm × 90 nm	0.0120	1.89	98

Thermal stability factors ($\Delta = E/k_BT$) for MTJs with varying lateral dimensions using free layer H_k extracted from HMR and $E = M_sH_kV/2$ are shown in Table I. Here, M_s was obtained to be 1000 emu/cm^3 from vibrating sample magnetometer measurements on unpatterned films and V is the free layer volume calculated from the nominal device dimensions. The thermal stability was seen to increase with area (i.e., volume of free layer), as well as having the expected significant dependence on aspect ratios (compare, e.g., thermal stabilities for 160 nm × 65 nm and 140 nm × 85 nm devices).

IV. CONCLUSION

We proposed and evaluated use of HMR curves for extraction of device-level anisotropy field and thermal stability of MTJ cells. Micromagnetic simulations revealed that misalignment in exchange bias on fixed layer and in-plane rotation of fixed layer cause HMR curves to deviate from those expected in the absence of such effects. We derived fitting functions incorporating these deviations in the single-domain approximation for a strongly pinned fixed layer when nonuniformity of the dipolar fields can be neglected, and applied them to calculate thermal stability factors for MTJs with varying lateral pillar dimensions.

[1]E. Chen, D. Apalkov, Z. Diao, A. Driskill-Smith, D. Druist, D. Lottis, V. Nikitin, X. Tang, S. Watts, S. Wang, S. A. Wolf, A. W. Ghosh, J. W. Lu, S. J. Poon, M. Stan, W. H. Butler, S. Gupta, C.K.A. Mewes, Tim Mewes, and P. B. Visscher, IEEE Trans. Magn. **46**, 1873 (2010).
[2]S. Ikeda, J. Hayakawa, Young Min Lee, F. Matsukura, Y. Ohno, T. Hanyu, and H. Ohno, IEEE Trans. Electron Devices **54**, 991 (2007).
[3]R. D. McMichel and M. D. Stiles, J. Appl. Phys. **97**, 10J901 (2005).
[4]A. A. Tulapurkar, Y. Suzuki, A. Fukushima, H. Kubota, H. Maehara, K. Tsunekawa, D. D. Djayaprawira, N. Watanabe, and S. Yuasa, Nature **438**, 339 (2005).; J. C. Sankey, P. M. Braganca, A.G.F. Gracia, I. N. Krivorotov, R. A. Buhrman, and D. C. Ralph, Phys. Rev. Lett. **96**, 227601 (2006).
[5]E. C. Stoner and E. P. Wohlfarth, Philos. Trans. R. Soc. London, Ser. A **240**, 826 (1948).
[6]C. Tannous and J. Gieraltowski, Eur. J. Phys. **29** 475 (2008).
[7]J. Z. Sun, J. C. Slonczewski, P. L. Trouilloud, D. Abraham, Ian Bacchus, W. J. Gallagher, J. Hummel, Yu Lu, G. Wright, S.S.P. Parkin, and R. H. Koch, Appl. Phys. Lett. **78**, 40004 (2001).
[8]R. V. Kohn, M. G. Reznikoff, and E. V. Eijnden, J. Nonlinear Sci. **15**, 223–253 (2005).
[9]M. R. Scheinfein, developer, LLG Micromagnetics Simulator, http://llgmicro.home.mindspring.com/.